4
Magnetic and Microwave Absorption Properties

This chapter describes about the magnetic properties of pristine and fluorinated hematite prepared by hydrothermal method. The fluorination was performed using fluorinating agents such as F-TEDA, HF, NaF and $TBABF_4$. The hysteresis loops were studied for all of the samples and the magnetizations versus temperature curves have been analyzed to understand the difference in the magnetic properties due to fluorination. This study is focused on the interplay between the fluorine content (varying fluorinating agents and F-TEDA concentration 0% to 40%) and resulting changes in the structural and magnetic properties. Material was further evaluated for its microwave absorption properties. The microwave absorption characteristics were studied by measuring real part and imaginary part of permittivity (Ɛ) and permeability (μ) both for pristine α-Fe_2O_3 and surface fluorinated Fe_2O_3 in the frequency range of 5.85-18 GHz. The chapter is composed of six sections and six sub-sections. The introduction of chapter is discussed in section 4.1. Structural characterizations are mentioned in section 4.3. The results and discussion of magnetic characterization techniques are expressed in the section 4.4. Microwave absorption properties are mentioned in section 4.5 and conclusion is discussed in the section 4.6.

4.1 INTRODUCTION

α-Fe_2O_3 is found to be antiferromagnetic in nature (Neel's temperature $T_N \approx 950$ K) that turns weakly ferromagnetic above a certain Morin temperature, $T_M \approx 263$ [Bhowmik and Saravanan, 2010]. This weak ferromagnetic behavior of α-Fe_2O_3 have been utilized in various applications such as detection of uric acid [Suresh et al., 2014], removal of dye from contaminated water [Ranjithkumar et al., 2014], heat transfer systems, as nano fluids [Rufus et al., 2016], lithium-ion batteries [B Wang et al., 2011], biomedical research [Narayanan and Han, 2016] and magnetic data storage. The magnetic properties of α-Fe_2O_3 are sensitive to crystallinity, morphology, and inter-particle interactions of the samples [Deraz and Alarifi, 2012; Panjan et al., 2012; Spasojević et al., 2006; Tadić et al., 2011; Teja and Koh, 2009]. For example, Cao et al. synthesized the dendritic structures of α-Fe_2O_3 and obtained a large coercive field of 1510 Oe with Morin transition at 216 K [Cao et al., 2005]. The coercivity of dendritic α-Fe_2O_3 nanostructures was found to increase with corresponding decrease in saturation magnetization upon conversion to snowflake type structure [Bharathi et al., 2010].

The magnetic properties of α-Fe_2O_3 are also adjusted by surface modification or by doping with metals and metal oxides. Surface coating of α-Fe_2O_3 nanowires with ZnO have resulted into high saturation magnetization due to uncompensated surface spins of ZnO shell [Sarkar et al., 2012]. An increase in coercivity with decrease in grain size was also reported in α-Fe_2O_3 and $CoFe_2O_4$ nano composites [Lv et al., 2015]. Different sources of fluoride anions such as HF, NaF, NH_4F and LiF was also used in literature for assisting the growth process as these act as shape directing agents by adsorbing on metal oxide surfaces. For example, Sun et al. synthesized dodecahedral and octahedral α-Fe_2O_3 with the aid of fluoride anions and reported different magnetic behavior [Lv et al., 2010].

Fluorinated α-Fe_2O_3 nanostructures undergo a significant increase in saturation magnetization with lowering of coercive field while increasing F-TEDA concentration. The results obtained with F-TEDA was compared with other fluoride ion sources such as hydrofluoric acid (HF), sodium fluoride (NaF), ammonium fluoride (NH_4F) and tetraethylammonium tetrafluoroborate ($TBABF_4$) as control. The other fluorinating agents have hardly any effect on magnetic properties. This study was further extended for finding the application of fluorinated hematite as radar absorbing material.

Radar absorbing materials (RAM) have attracted considerable attention in recent past for their key role in imparting stealth features to various combat military targets such as fighter aircrafts, tanks, ships, etc. The performance of a radar absorbing material can be defined in terms of bulk macroscopic interaction process such as permittivity and permeability. The electromagnetic parameters defining the suitability of a given material depend on its dielectric and magnetic characteristics i.e. imaginary and real part of permittivity (Ɛ) and permeability (μ). Both of these components can be represented by complex numbers. The imaginary part is associated with the loss or absorption in the material as shown in equation 4.1 & 4.2.

$$\varepsilon_r = \varepsilon_r' - j\varepsilon_r'' \quad (4.1)$$

$$\mu_r = \mu_r' - j\mu_r'' \quad (4.2)$$

Where, ε_r' & μ_r' represents real parts of permittivity and permeability, respectively; whereas ε_r'' & μ_r'' represents imaginary parts of permittivity and permeability, respectively.

The important characteristics of an ideal RAM include their low density, high stability & integrity over a broad temperature range besides high absorption over broad frequency and low cost [Vinoy and Jha, 1995]. Iron oxide materials were also studied for RAM application. Polyaniline/γ-Fe_2O_3 nano composite were synthesized and reported for their Microwave (MW) absorption in the range of 13.4 and 16 GHz [Wang et al., 2008]. Sun et al. reported microwave absorption of iron nano particles in the range of 2-9 GHz. The material, Fe_3O_4, γ-Fe_2O_3 was prepared by red-ox process from dendritic α-Fe_2O_3 [Sun et al., 2011].

As such, α-Fe_2O_3 possess poor microwave absorption characteristics due to nonmagnetic nature[Brezesinski et al., 2006]. Any improvement in microwave absorption by hematite is considered important. Therefore, in addition to magnetic properties measurements, this chapter also deals with the microwave absorption studies of surface fluorinated α-Fe_2O_3 and their comparison with pristine α-Fe_2O_3.

4.2 MATERIAL SYNTHESIS

In-situ fluorination was carried out for synthesis of fluorinated α-Fe_2O_3. The reaction was performed in Teflon lined hydrothermal vessel. Five fluorinating agents as depicted in Figure 4.1 were used for employing fluorine into α-Fe_2O_3. Among these fluorinating agents, F-TEDA is a source of fluoronium ion (F^+) whereas the rest of fluorinating agents produces Fluoride (F^-) ion in aqueous reaction medium. The $K_3[Fe(CN)_6]$ was used as iron precursor for all fluorinating agents. $TBABF_4$ was chosen for finding the contribution of fluoronium ion of F-TEDA since counter ion of $TBABF_4$ and F-TEDA is same. The nature of F^+ was also compared with F^- by using H^+F^-, $NH_4^+F^-$, Na^+F^- as different fluorinating agents. The fluorination reactions were performed as per details enlisted in Table 4.1.

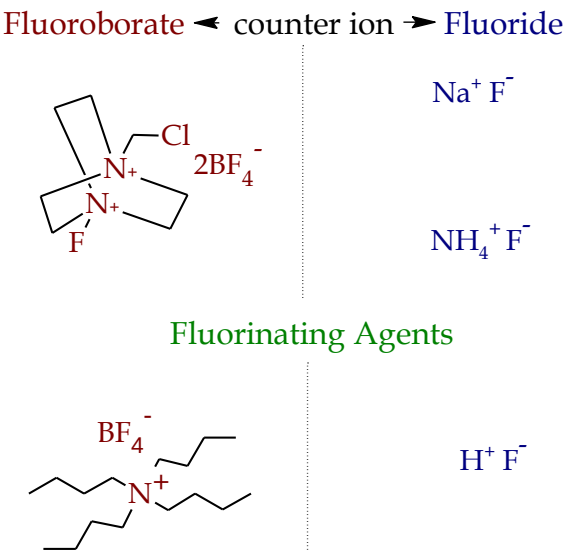

Figure 4.1: Structure of fluorinating agents used for in-situ fluorination of α-Fe_2O_3

Table 4.1: List of synthesized fluorinated α-Fe_2O_3 samples

S.No.	*Fluorinating agent %*	*Fluorinating agent, Quantity*	*Fe precursor $K_3[Fe(CN)_6]$*	*Product formed*
1.	Nil	NIL	(15 mM) 1.23 g	α-Fe_2O_3
2.	Selectfluor (F-TEDA)	10% wt., 0.123 g	(15 mM) 1.23 g	F-TEDA-10%
3.		20% wt., 0.246 g	(15 mM) 1.23 g	F-TEDA-20%
4.		30% wt., 0.369 g	(15 mM) 1.23 g	F-TEDA-30%
5.		40% wt., 0.492 g	(15 mM) 1.23 g	F-TEDA-40%
6.	Hydrofluoric acid	20% wt., 246 µL	(15 mM) 1.23 g	HF-20%
7.	Sodium fluoride	20% wt., 0.246 g	(15 mM) 1.23 g	NaF-20%
8.	Tetrabutyl ammonium tetrafluoroborate	20% wt., 0.246 g	(15 mM) 1.23 g	$TBABF_4$-20%
9.	Ammonium fluoride	20% wt., 0.246 g	(15 mM) 1.23 g	NH_4F-20%

4.3 PHYSICAL CHARACTERIZATION

The physical characterization of samples obtained from various fluorinating agents and iron precursor was carried out to assess crystal structure and morphology of samples. X-ray diffraction and electron microscopy were used for revealing the relevant information. The characterization data and their analysis are presented in sub-sections from 4.3.1 to 4.3.2 as following:

(4.3.1) *X-ray diffraction* gave information about crystal structure and phase formation.

(4.3.2) *Electron microscopy* provided information about morphology of samples.

4.3.1 X-ray Powder Diffraction Analysis

The X-ray pattern corresponding to different fluorinating agents is presented in Figure 4.2. The spectra were recorded for iron oxides synthesized by using 20% wt. of fluorinating agents with respect to iron precursor. The obtained patterns resembles with pristine α-Fe_2O_3 and rhombohedra structure of hematite (JCPDS data card number 86–0550) [Congiu et al., 2017]. It can be seen from the curves that there is no emergence of any new peak except minor impurity peak in case of HF. This signifies that different fluorinating (F-TEDA, HF, NH_4F, NaF and $TBABF_4$) agents do not alter the crystalline structure and phase of α-Fe_2O_3. However, the orientation of α-Fe_2O_3 along (104) and (110) plane has influence of systematic addition of HF

and F-TEDA. The intensity of (104) and (110) plane decreases in case of HF (Figure 4.2). However, in case of F-TEDA, systematic increase of (110) peak was observed (Figure 4.3). This implied that HF acts as itching agent in the crystallization process of hematite whereas F-TEDA acts as growth directing agent. The increase in (110) peak in case of F-TEDA is attributed to growth along {11$\bar{2}$0} plane. $TBABF_4$ and NaF have not shown any considerable change in X-ray diffraction peak of sample. NH_4F has relatively higher ratio of (110) as compared to $TBABF_4$ and NaF.

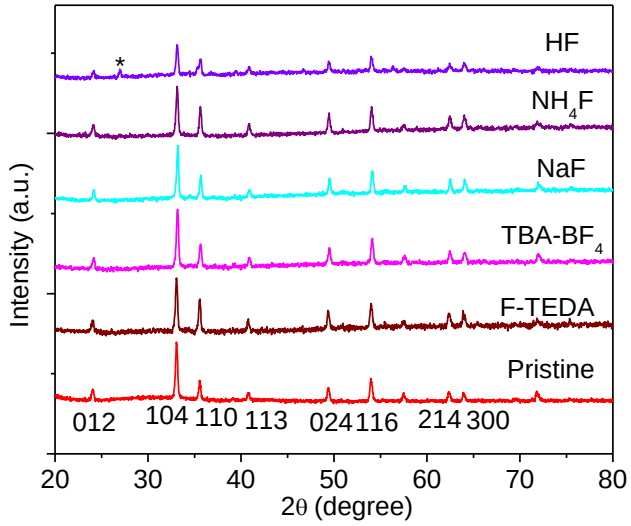

Figure 4.2: X-ray pattern of α- Fe_2O_3 and F- α- Fe_2O_3 synthesized using 20%wt. of fluorinating agents and * represents impurity peak

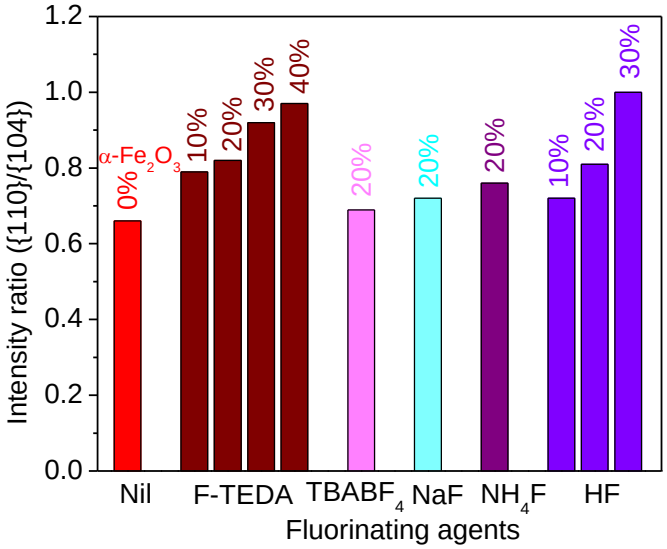

Figure 4.3: Intensity ratio of (110) and (104) plane in α- Fe_2O_3 and F- α- Fe_2O_3 synthesized with different fluorinating agents. Percentage represents the wt. % quantity of fluorinating agents used with respect to Fe precursor

The crystallite sizes α-Fe_2O_3 and fluorinated α-Fe_2O_3 samples were also calculated using Scherrer equation. The results are presented in Table 4.2. It is hard to evidence any systematic variation in crystallite size of samples synthesized using F-TEDA, $TBABF_4$, NH_4F and NaF. It was observed that crystallite size of different wt. % HF mediated samples decreases due to itching.

Table 4.2: Crystallite size of α-Fe_2O_3 and fluorinated α-Fe_2O_3 samples calculated using (110) and (104) planes.

Fluorinating agents	*Crystallite size, nm (110)*	*Crystallite size, nm (104)*	*Crystallite size, nm mean*
Pristine α -Fe_2O_3	30.9	33.3	32.1
F-TEDA	31.1	32.8	32.0
$TBABF_4$	30.6	34.4	32.5
NaF	30.6	31.3	30.9
NH_4F	29.5	31.5	30.5
HF	27.9	30.1	29.0

4.3.2 Scanning Electron Microscope (SEM) Analysis

SEM images in Figure 4.4 (a-f) reveal the differences in the morphology and size resulting from the fluorination reactions which were performed under identical hydrothermal conditions. The relative size of dendrites increases in presence of F-TEDA signifying high growth rates. The increase in dendritic size in case of F-TEDA may be attributed to the presence of fluoronium (F^+) ions which facilitate the growth mechanism. In case of $TBABF_4$ and NaF, the dendrites obtained were similar to pristine α-Fe_2O_3, which was synthesized without using any fluorinating agent. Therefore, $TBABF_4$ and NaF are acting as neutral agents without affecting the growth of α-Fe_2O_3.

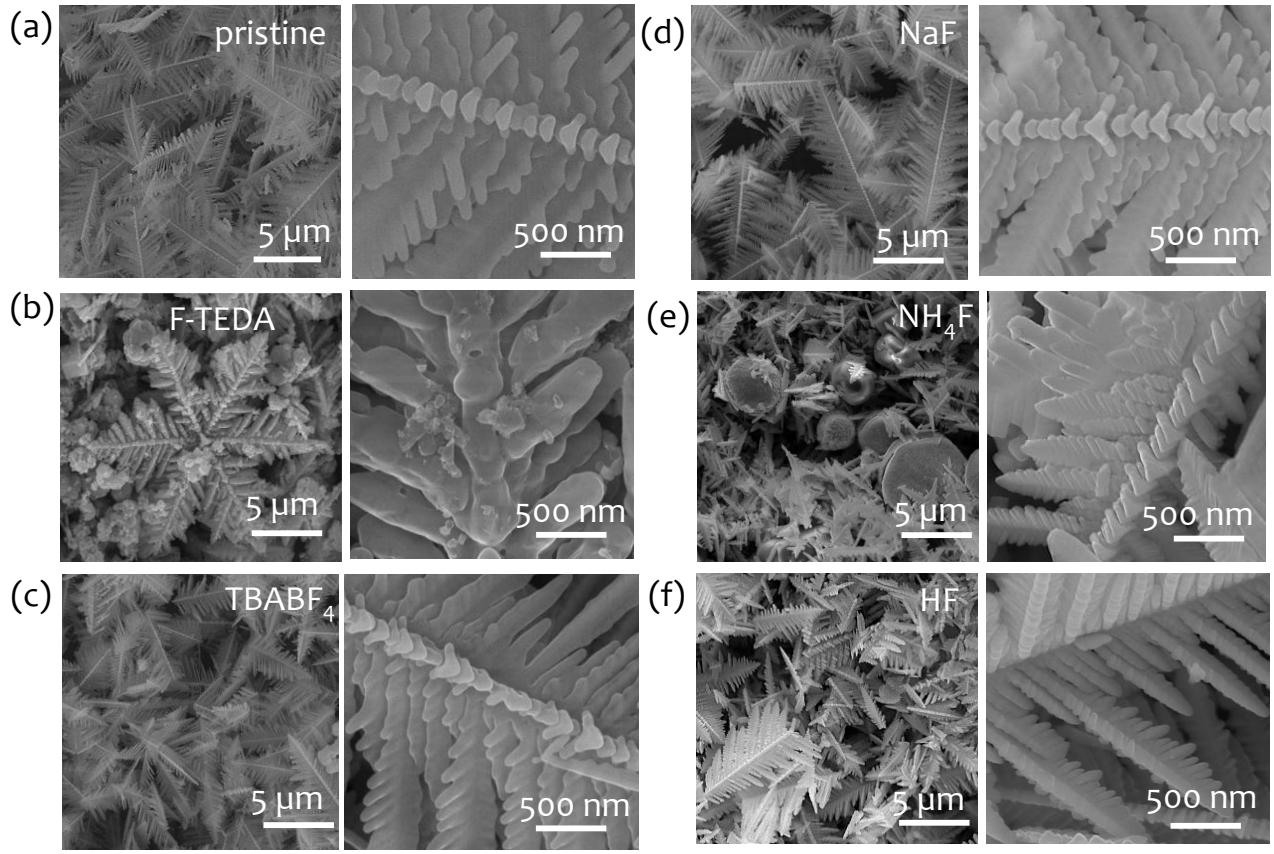

Figure 4.4: SEM images of (a) pristine α-Fe_2O_3, (b) F-TEDA, (c) $TBABF_4$, (d) NaF, (e) NH_4F, and (f) HF mediated F-α-Fe_2O_3 synthesis (20wt. % were used with respect to Fe precursor)

However, in case of NH_4F and HF the dendrites are appeared to sharper and shorter. This may be attributed to the strong coordinating tendency of F^- ions with Fe atoms on (110) and

due to corrosive nature of HF. The presence of NH_4F also resulted in mixed morphology of spherical and dendrites. Therefore, it is clear that the difference in growth mechanism is due to electrophilic fluorine that leads to directional growth of α-Fe_2O_3 whereas nucleophilic fluorine act as etching agent and may be inhibiting the self-aggregation and further growth. Interestingly, in case of F-TEDA (20 wt. %), the morphological progression along (110) orientation takes place resulting in six fold symmetry (Figure 4.4b). The fluorine content of this batch was estimated by EDS analysis. F-TEDA- 20% shows fluorine content of ~2.08 wt. % in α-Fe_2O_3 whereas no fluorine was detected for α-Fe_2O_3 synthesized with HF, NH_4F, NaF and $TBABF_4$. Probably, fluorine content was too low to be detected by EDS studies in these materials. A maximum fluorine content of 3.69 wt% was obtained for 30% F-TEDA while it decreased to 2.27% in case of 40% F-TEDA. The decrease in fluorine content at 40% F-TEDA could be due to drastic changes in surface morphology hindering the surface adsorption of the fluorine at all planes resulting in a decrease in the fluorine content.

4.4 MAGNETIC CHARACTERIZATION OF SURFCE FLUORINATED HEMATITE

The magnetic characterization of hematite and surface fluorinated hematite was performed to obtain the magnetization curve and Morin transition temperature. These characterization data and their analysis are presented in sub-sections from 4.4.1 to 4.4.2 as following:

(4.4.1) *M-H Measurements*

(4.4.2) *M-T Measurements*

4.4.1 M-H Measurements

Magnetic measurements were performed by SQUID magnetometer. M-H curves were recorded in the field range ± 10,000 O_e at temperature of 300 K. The M-H measurements were subtracted with diamagnetic contribution of the sample holder. The magnetic measurement results of α-Fe_2O_3 and F-α-Fe_2O_3 are presented in Figure 4.5.

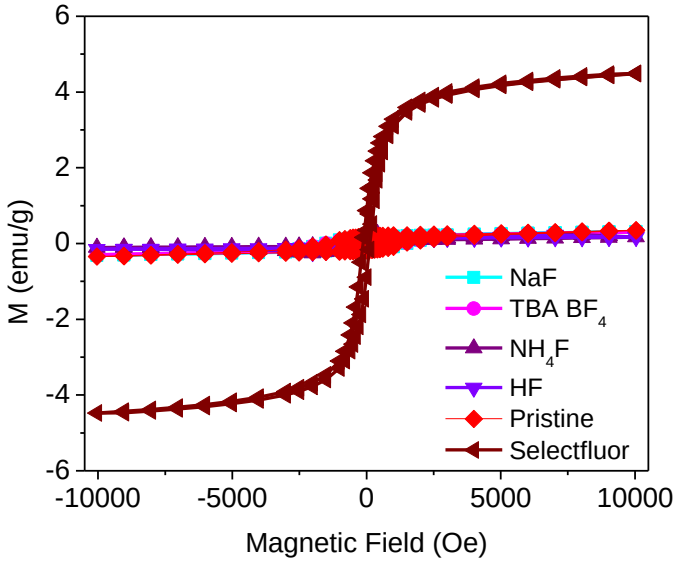

Figure 4.5: Magnetic hysteresis loops (M-H curves) of pristine α-Fe_2O_3, F-TEDA, $TBABF_4$, NaF, NH_4F, and HF mediated F-α-Fe_2O_3 (20wt. % of fluorinating agent were used with respect to Fe precursor)

Magnetic parameters such as coercivity (H_c), and residual magnetization values (M_r) and saturation magnetization (M_s) were calculated from the M-H data. The M-H data of pristine α-Fe_2O_3 shows characteristic hysteresis with low magnetization. The α-Fe_2O_3 synthesized in presence of fluorinating agents such as HF, NH_4F, $TBABF_4$ and NaF possess magnetization values close to α-Fe_2O_3. However, α-Fe_2O_3 synthesized with F-TEDA displayed remarkable

changes in magnetic property. The total anisotropy constant, ($K_p = \frac{M_s}{M_r}$) increases by nearly three order of magnitude and reaches to 5.21 from 1.8 × 10^{-3} (for pristine α-Fe_2O_3) with addition of F-TEDA (Table 4.3). Additionally, there is an approximately 10 times lower coercivity (124.55 O_e) and 13 times higher saturation magnetization (4.4 O_e) observed in 20 wt. % F-TEDA sample. The changes in these values clearly indicate improved ferromagnetic behavior for the F-TEDA fluorinated α-Fe_2O_3 at room temperature. The large magnetic moment of F-TEDA mediated F-α-Fe_2O_3 may have contributions from both the uncompensated surface spins and canting of the sub-lattice spins. This anomalous behavior could be due to replacement of the surface adsorbed OH^- ions by fluoride ions from F-TEDA [Bharathi et al., 2010].

Table 4.3: M-H data for α-Fe_2O_3 synthesized with different fluorinating agents using 20 wt. %.

S.No.	Sample	$H_C(O_e)$ at 300 K	M_r(emu/g) at 300 K	M_S(emu/g) at 300 K	$K_p = \frac{M_s}{M_r}$
1.	Pristine α-Fe_2O_3	959	0.18	0.38	0.0018
2.	F-TEDA	124	0.86	4.46	5.22
3.	NaF	1500	0.16	0.32	1.93
4.	$TBABF_4$	1500	0.16	0.29	1.87
5.	HF	1203	0.13	0.22	1.73
6.	NH_4F	1140	0.08	0.25	3.04

For further understanding the interesting and remarkable magnetic property exhibited by F-TEDA mediated F-α-Fe_2O_3, other samples of F-TEDA as fluorinating agent, such as 10% wt., 30% wt. and 40% wt. were also examined. The results are figured in Figure 4.6.

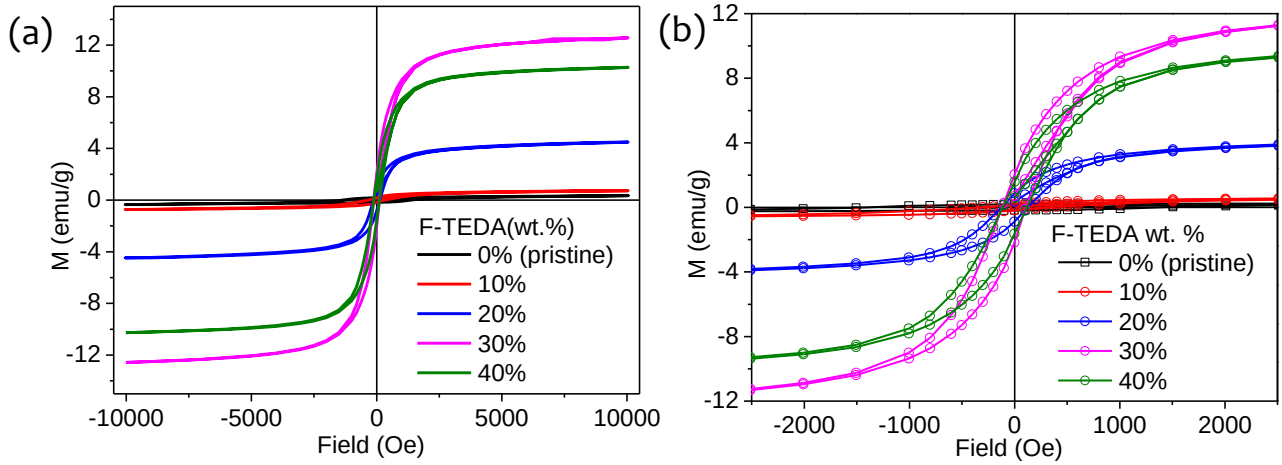

Figure 4.6: M-H curve of hematite and fluorinated hematite (fluorinated with different wt. % F-TEDA)

The saturation magnetization increases with increasing wt. % of F-TEDA in the reaction medium. The values are presented in Table 4.4. The maximum observed saturation magnetization value was 14.04 emu/g at 30% wt. of F-TEDA with respect to Fe precursor. The further increase in F-TEDA concentration has decreased saturation magnetization. However, there is no significant change in coercivity beyond 10% wt. of F-TEDA. The improved value of

saturation magnetization at high F-TEDA concentration may be due to an increase in the surface spins of fluorine layer that induce moments through exchange coupling between the interface surface spin and the core spin of Fe_2O_3, thus enhancing the overall magnetization.

Table 4.4: M-H data for α-Fe_2O_3 and F- α-Fe_2O_3 synthesized with different wt. % of F-TEDA

S.No.	Sample	H_c (O_e) 300 K	M_r(emu/g) 300 K	M_s(emu/g) 300 K	$K_p = \frac{M_s}{M_r}$
1.	Pristine α-Fe_2O_3	959	0.18	0.34	0.0018
2.	F-TEDA-10%	135	0.17	0.72	4.18
3.	F-TEDA-20%	124	0.86	4.46	5.22
4.	F-TEDA-30%	115	0.72	12.58	17.33
5.	F-TEDA-40%	109	1.58	10.23	6.48

The relation of saturation magnetization and coercivity with fluorine at.% for different percentages of F-TEDA is shown in Figure 4.7.

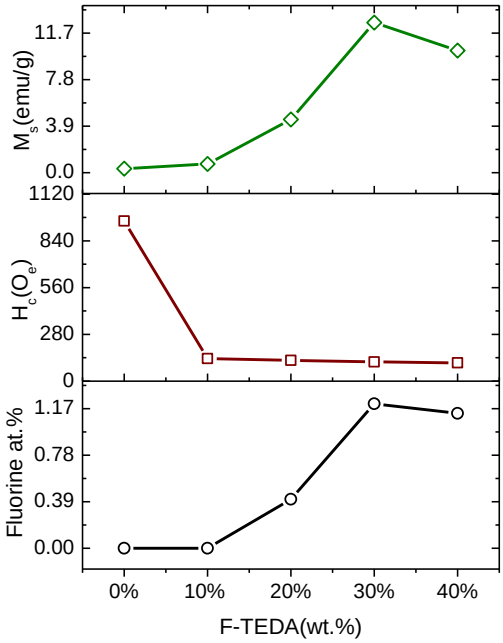

Figure 4.7: Fluorine at.% in F- α-Fe_2O_3 mediated by different wt.% of F-TEDA in relation with H_c and M_s

4.4.2 M-T Measurements

The bulk Hematite shows Morin transition (antiferromagnetic to weakly ferromagnetic transition) at 260 K. To understand the effect of fluorination by different fluorinating agents on Morin transition temperature of α-Fe_2O_3, zero-field cooled (ZFC) and field-cooled (FC), magnetization was performed from 20 K to 300 K for all the samples in a field of 500 O_e.

Briefly, in the process of ZFC the samples were first cooled in zero-field down to 20K and then the required field was applied and the obtained data are denoted as ZFC. Whereas, in FC mode the samples were first cooled in the presence of applied field then data were collected as the temperature was increased from 20 K to 300 K. At room temperature the magnetic field

keeps the spins oriented and if the material is cooled in the applied field then the oriented spins have less chance to disorient.

Therefore, under this (magnetic field) condition magnetic saturation is attained. ZFC and FC curves can give the information of para-magnetism, signature of spin-glass behavior, presence of exchange bias and superconducting properties.

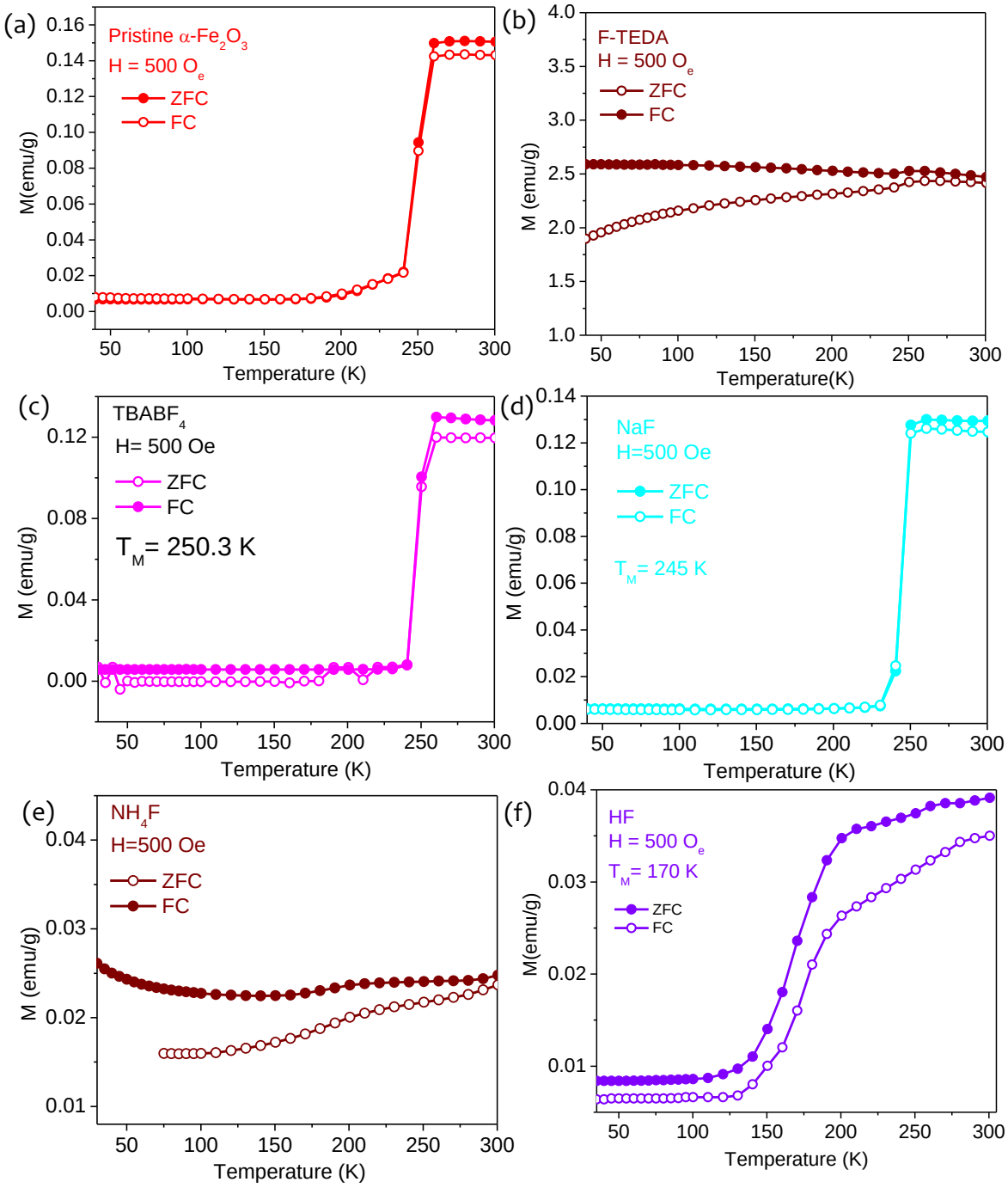

Figure 4.8: Zero-field cooled and field cooled magnetic measurements at 500 O_e applied filed for (a) Pristine Fe_2O_3 (b) F-TEDA (c) $TBABF_4$ (d) NaF (e) NH_4F and (f) HF

As depicted in Figure 4.8a pristine α-Fe_2O_3 shows sharp transition from antiferromagnetic to weakly ferromagnetic at T_M = 250.4 K. This lower side shifting of T_M of pristine α-Fe_2O_3 as compared to bulk α-Fe_2O_3 may be attributed to its dendritic nanostructure [Xing et al., 2009]. In case on F-TEDA mediated F- α-Fe_2O_3 (Figure 4.8b) the T_M was found to be

lower (245 K) as compared to pristine α-Fe_2O_3. This may be due to presence of fluoride which might be reducing interparticle interaction. Interestingly, the net magnetic moment was recorded high even at low temperature indicating the alignment of spin at low temperature. HF mediated samples (Figure 4.8f) shows T_M at 170 K with low value of magnetization and it may be caused by itching effect of HF on dendritic crystallites without any fluorination. $TBABF_4$ and NaF showed similar behavior of Morin transition with respect to pristine α-Fe_2O_3 as there are hardly any changes in structure or morphology of dendrites. The ZFC and FC curves of $TBABF_4$ and NaF curves are depicted in Figure 4.8c and 4.8d respectively. The NH_4F curve (Figure 4.8e) shows similarity with F-TEDA samples. However, the value of saturation magnetization was low due to absence of any fluorine content into samples. Therefore, the ZFC and FC behavior also corroborated with presence of fluorine content and morphology.

The temperature dependent ZFC and FC magnetization curves are displayed for different percentages of F-TEDA (Figure 4.9). It is evident from the curve that splitting of ZFC and FC increases with higher F-TEDA wt.% while the Morin transition is getting suppressed systematically. The suppression in Morin transition may be attributed form possible lattice strain and defects induced by surface fluorination on α-Fe_2O_3 dendrites [Cao et al., 2005].

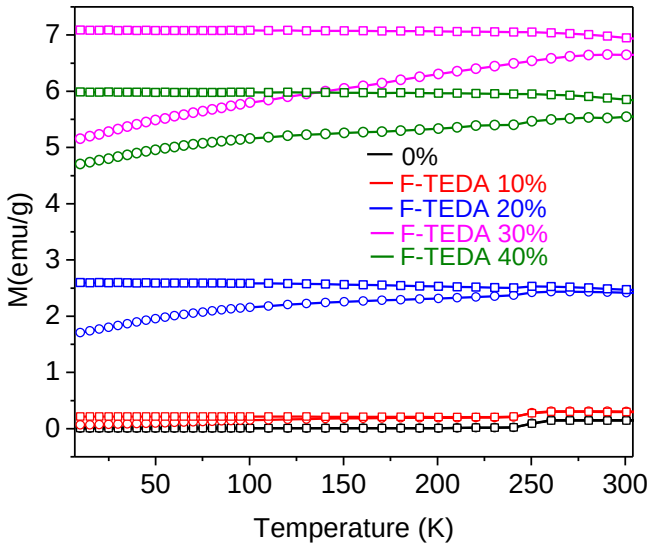

Figure 4.9: Temperature dependent magnetization of α- Fe_2O_3 and F- α-Fe_2O_3 (at 500 O_e) synthesized at different wt. % of F-TEDA

It is an interesting and first ever observation about the magnetization of α-Fe_2O_3 fluorinated with F-TEDA 30% wt. It may be attributed to contributions from both the canting of the sub-lattice spins (weak ferromagnetism) along with uncompensated surface spins [Kim et al., 2006]. The experiments were further extended for microwave absorption measurement. The driving force for consideration of microwave absorber is certainly the noticeable value of saturation magnetization upon fluorination.

4.5 MICROWAVE ABSORPTION PROPERTIES

An HP8510C network analyzer was used to carry out transmission and reflection loss measurements in the C, X and Ku bands in the microwave frequency. Magnetic loss tangent ($\tan \delta_\mu = \mu_r''/\mu_r'$) of the materials were calculated from measured permeability values, over 6–18 GHz frequency range, using the Nicolson–Ross–Weir (NRW) algorithm [Chen et al., 2004].

These characterization data and their analysis are presented in sub-sections from 4.5.1 to 4.5.2 as following:

(4.5.1) *Microwave measurements*

(4.5.2) *Microwave reflection loss measurements*

4.5.1 Microwave Measurements

Microwave measurements for frequency-dependent permeability (μ) and permittivity (ε) were carried out on HP8510C network analyzer. The real and imaginary parts of permeability, (μ_r', μ_r'') and permittivity (ε_r', ε_r'') values were calculated using S parameters and variation with respect to frequency are represented in Figure 4.10a & b, whereas the loss parameters (($tan\ \delta_\varepsilon$, ratio of ε_r'' & ε_r') and ($tan\ \delta_\mu$, ratio of μ_r'' & μ_r')) quantify the MW inside the material, are shown in Figure 4.10c & d.

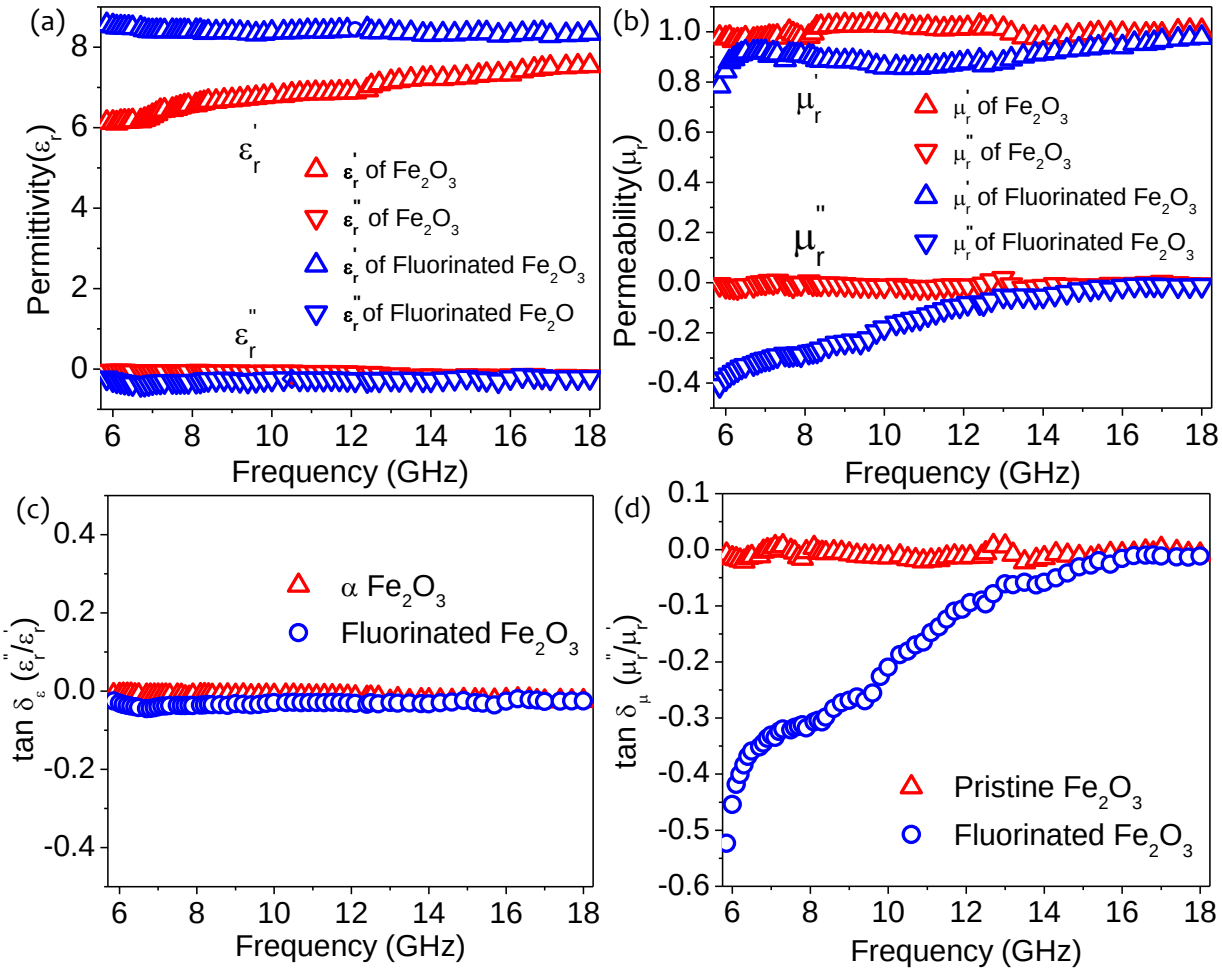

Figure 4.10: Real and imaginary permittivity (a), permeability (b), dielectric loss (c) and magnetic loss (d) for α-Fe_2O_3 and F- α-Fe_2O_3 samples over 6–18 GHz

As shown in the Figure 4.10a there is negligible change in the imaginary part of permittivity values with change in frequency for both the samples. However, there is slight change in the real permittivity values of α-Fe_2O_3 sample with negligible frequency dependent change in real part of permittivity of the surface fluorinated Fe_2O_3. On the other hand, in case of pure α-Fe_2O_3 there is negligible frequency dependent change in the real and imaginary part of permeability. However, fluorinated Fe_2O_3 shows dispersive behaviour; its imaginary permeability (μ_r'') value change in the range of -0.41 to -0.011 corresponding to the frequency range of 5.85 GHz- 18 GHz (Figure 4.10b). The imaginary part of permeability, which is responsible for MW energy loss, depends on saturation magnetization (M_S) and coercive field (H_C) as given in following equation number 4.3.[Chen and Gu, 2012]

$$\mu_r'' = \frac{M_S^2}{4\mu_0 K_1 \alpha} \propto \frac{M_S^2}{H_c} \qquad (4.3)$$

Where, M_S is saturation magnetization, μ_0 is permeability of vacuum, K_1 is anisotropic

constant, α is Gilbert damping coefficient and H_C is a coercive field. Upon fluorination, α-Fe_2O_3 undergoes an antiferromagnetic to ferromagnetic transition with saturation magnetization value of ≈13 emu/g and coercivity of 109.8 Oe. [Bahuguna et al., 2017; Kim et al., 2006] Therefore, M_S values of fluorinated Fe_2O_3 shows an increasing trend in comparison to pristine Fe_2O_3 sample. As a result μ_r'' values are found to increase in the fluorinated Fe_2O_3 sample. Figure 4d shows the calculated frequency dependent magnetic loss tangent over 5.85–18 GHz. Hence, the microwave absorption of fluorinated Fe_2O_3 is mainly due to its magnetic loss characteristics. The magnetic loss in fluorinated Fe_2O_3 may be attributed to higher saturation magnetization values as compared to pristine α- Fe_2O_3.

4.5.1 Microwave Reflection Loss Measurements

Based on these measured EM parameters of the material, the thickness dependent MW reflection losses (RL) of fluorinated Fe_2O_3 was calculated using $Z_{in} = Z_0\sqrt{(\mu_r/\varepsilon_r)}\ tanh(\gamma t)$ equation [Michielssen et al., 1993; Naito and Suetake, 1971] and illustrated in Figure 4.11., Z_{in} is input impedance, Z_0 is characteristic impedance of vacuum, $Z_0 = (\sqrt{(\mu_0/\varepsilon_0)})$ having a value of 377 Ω, ε_0 is dielectric constant and μ_0 is permeability of free space, $\gamma = j\omega\sqrt{\mu_r\varepsilon_r/c}$ is the propagation factor in the material, ω is the angular frequency, c is the speed of light and t is the thickness of the absorber. Absorption in decibels (dB) can be written as $RL(dB) = -20\ log_{10}|Z_{in} - Z_0/Z_{in} + Z_0|$[Meshram et al., 2004]. Fluorinated sample shows enhanced absorption towards lower frequency side. The effective reflection loss of more than 5dB could be achieved over a frequency range 6-12 GHz while varying thickness from 2.5 mm to 3.5 mm. The maximum RL value of ≈ -18dB was observed at 7.5 GHz for thickness ≈3.5 mm which is promising for RAM application.

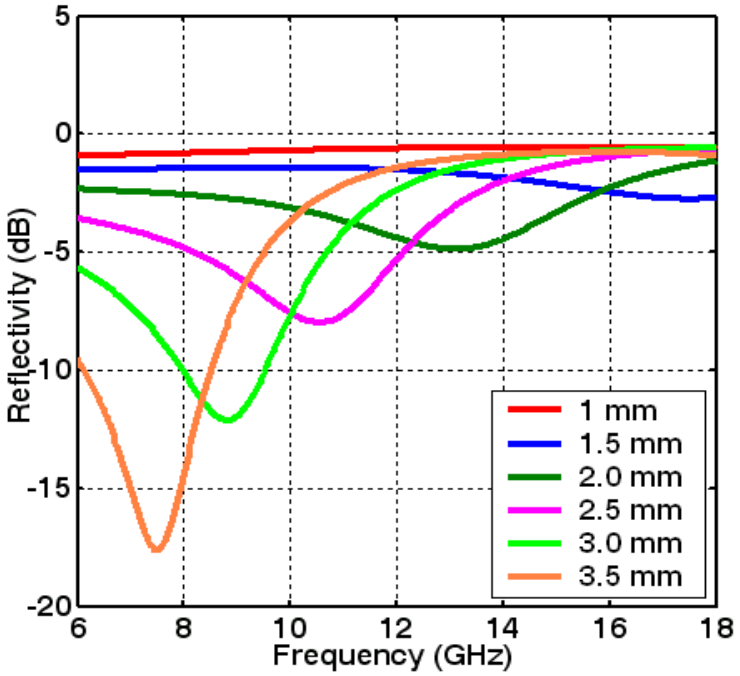

Figure 4.11: Simulated absorption characteristics for fluorinated Fe_2O_3 at different thicknesses

The developed RAM has to be applied on a metallic body for its application. To determine the reflectivity reduction performance of the material, simulation of reflectivity has been carried out by backing the material layer with PEC (Perfect electric conductor). The simulation of reflectivity response utilizes the measured complex permittivity and permeability parameters and thickness of material. The reflectivity response can be tuned by changing the thickness of material layer i.e., the loss-bandwidth can be tuned as per requirement. As shown in Figure 4.11, the thickness of 2.5 mm provides 5 dB loss for complete X-band, thickness of 3.0 mm covers 6-11 GHz for 5 dB loss. Similarly the same material can be used at different

frequency ranges as per requirement by tuning the thickness of material. The actual measurements of reflection loss can be carried out in an anechoic chamber facility. The same requires larger size samples and will be carried out in future work. However, since the Reflectivity simulations are carried out using measured complex permittivity and permeability parameters; the simulation results are good enough to ensure that the material is highly useful as a RAM (schematic Figure 4.12).

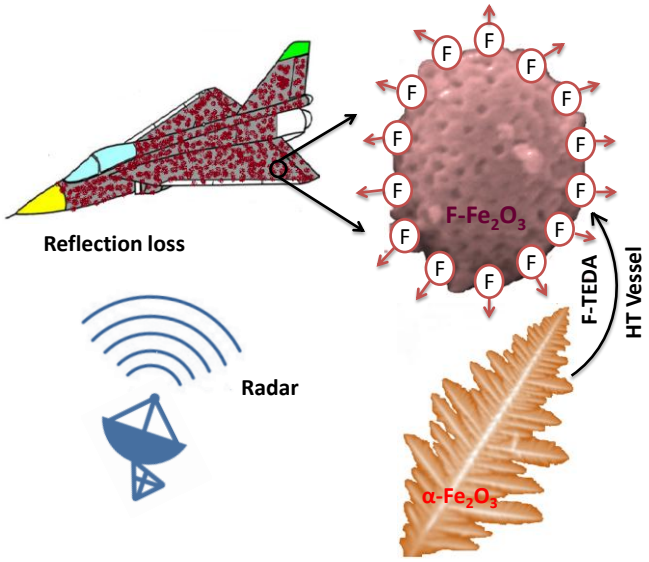

Figure: 4.12: Schematics of fluorinated hematite being used for microwave absorption material

4.6 CONCLUSION:

In summary, the fluorination of α-Fe_2O_3 changes the magnetic characteristics of α-Fe_2O_3. The saturation magnetization increased considerable upon fluorinating with F-TEDA. 30 wt.% of F-TEDA was found to be optimum value for introducing 37 times more M_s value as compared to pristine α-Fe_2O_3. The same behavior was not observed with other fluorinating agents. The Fluorinated α-Fe_2O_3 was explored for microwave absorption properties. The changed saturation magnetization values in fluorinated hematite thereby, inducing in it absorption at a broad range of microwave frequencies. Though the quantum of absorption may not be very high as compared to γ- Fe_2O_3 or spinal ferrite; but it is first of its kind study for microwave absorption over the broad frequency range (5.85 to 18 GHz) for any surface modified hematite.

It also opens new research opportunities to explore the potential of surface modified readily available α-Fe_2O_3 as radar absorbing materials. Further, there is a scope of improvement by imparting permittivity loss part by using dielectric materials along with F-Fe_2O_3 as one of the ingredient.